Journal of Radiation Research, 2012, 53, 999–1005
doi: 10.1093/jrr/rrs048 Advance Access Publication 21 August 2012

Evaluation of beam hardening and photon scatter by brass compensator for IMRT

Shimpei HASHIMOTO[1,2,*], Katsuyuki KARASAWA[1], Yukio FUJITA[3], Hisayuki MIYASHITA[2], Weishan CHANG[2], Toru KAWACHI[4], Tetsurou KATAYOSE[5], Nao KOBAYASHI[2], Etsuo KUNIEDA[6] and Hidetoshi SAITOH[2]

[1]Tokyo Metropolitan Cancer and Infectious diseases Center Komagome Hospital, Honkomagome 3-18-22, Bunkyo-ku, Tokyo 113-8677, Japan
[2]Graduate School of Human Health Sciences, Tokyo Metropolitan University, Higashiogu 7-2-10, Arakawa-ku, Tokyo 116-8551, Japan
[3]Tohoku University, Seiryocho 2-1, Aoba-ku, Sendai 980-8575, Japan
[4]Chiba Cancer Center, Nitona-chou 666-2, Chuo-ku, Chiba 260-8717, Japan
[5]Association for Nuclear Technology in Medicine, Toranomon 1-8-16, Minato-ku, Tokyo 105-0001, Japan
[6]Tokai University, Shimokasuya 143, Isehara 259-1193, Japan
*Corresponding author. Tel: +81(3)3823-2101; Email: s.hashimoto@cick.jp

(Received 28 September 2011; revised 14 May 2012; accepted 12 June 2012)

When a brass compensator is set in a treatment beam, beam hardening may take place. This variation of the energy spectrum may affect the accuracy of dose calculation by a treatment planning system and the results of dose measurement of brass compensator intensity modulated radiation therapy (IMRT). In addition, when X-rays pass the compensator, scattered photons are generated within the compensator. Scattered photons may affect the monitor unit (MU) calculation. In this study, to evaluate the variation of dose distribution by the compensator, dose distribution was measured and energy spectrum was simulated using the Monte Carlo method. To investigate the influence of beam hardening for dose measurement using an ionization chamber, the beam quality correction factor was determined. Moreover, to clarify the effect of scattered photons generated within the compensator for the MU calculation, the head scatter factor was measured and energy spectrum analyses were performed. As a result, when X-rays passed the brass compensator, beam hardening occurred and dose distribution was varied. The variation of dose distribution and energy spectrum was larger with decreasing field size. This means that energy spectrum should be reproduced correctly to obtain high accuracy of dose calculation for the compensator IMRT. On the other hand, the influence of beam hardening on k_Q was insignificant. Furthermore, scattered photons were generated within the compensator, and scattered photons affect the head scatter factor. These results show that scattered photons must be taken into account for MU calculation for brass compensator IMRT.

Keywords: Brass compensator IMRT; beam hardening; dose distribution; quality correction factor; scatter photon

INTRODUCTION

Intensity modulated radiation therapy (IMRT) has come into wide use recently [1]. As a means of intensity modulation, the multileaf collimator (MLC) or compensation filter (compensator) is utilized [2]. The compensator technique has multiple advantages in comparison with the MLC technique [3]. Intensity modulation can be performed with higher resolution and smoother dose distribution, in consequence problems originating from patient movement can be minimized. Furthermore, the monitor unit (MU) can be reduced because multiple segments are unnecessary [4]. Production of a compensator used to be a troublesome job, however outside supply and delivery systems are available nowadays. Therefore compensator IMRT has become a realistic possibility.

With brass compensator IMRT, the photon energy spectrum can be varied downstream of the compensator because of beam hardening or softening. In the dose calculation using the convolution/superposition algorithm, the effective attenuation coefficient and dose kernel may be changed for calculation of TERMA and dose distribution. And in the absorbed dose measurement, the quality correction factor for the ionization chamber may be changed.

Furthermore, when X-rays pass the compensator, scattered photons can be generated within the compensator. These scattered photons should affect the head scatter factor for monitor unit calculation. Although many reports related to dose calculation and dosimetry for MLC IMRT have been published [5–11], there are few reports about brass compensator IMRT [12].

In this report, to evaluate the influence on dose distribution of the brass compensator, the difference in dose distribution was measured and simulated using the Monte Carlo method, and the influence of beam hardening or softening on dosimetry and dose calculation was evaluated. Furthermore, head scatter factor was measured and simulated in order to clarify the effect of scattered photons generated within the compensator.

MATERIALS AND METHODS

Depth dose measurement

In order to evaluate change of depth dose distribution by the brass compensator, percentage depth doses (PDDs) were measured for several field sizes and thicknesses of brass slab compensator (60% copper, 40% inc, $\rho = 8.37$ g cm^{-3}). The slab compensator was mounted on a blocking tray at a distance of 64.2 cm from the target of the 6-MV linear accelerator (Clinac 21EX, Varian, Palo Alto, US). PDD measurement was performed using the automated water phantom system (Blue Phantom, IBA, Schwarzenbruck, Germany) and ionization chamber (CC13, IBA).

Energy spectrum simulation

To analyze the photon spectrum varied by the compensator, energy spectra were simulated using the Monte Carlo method. The treatment head was reconstructed on the BEAMnrc simulation code [13–16] with conscientious geometry and material information provided by the manufacturer. Simulation parameters were optimized in order to reproduce actual dose distribution, and reproducibility was confirmed by agreement between measured and simulated dose distributions during the first step of the Monte Carlo procedure [6]. Several thicknesses of slab compensator were mounted on the treatment head and the energy of particles was sampled in the air and in a 10 cm depth of water.

Beam quality correction factor k_Q

To estimate the variation in ionization chamber sensitivity by beam hardening, the beam quality correction factor, k_Q, for four ionization chambers with wall materials consisting of PMMA (TN30013, PTW, Freiburg, Germany), graphite (2505/3,3A, Nuclear Enterprises, Beenham, UK), A-150 (2581, Nuclear Enterprises) and C-552 (PR-06C, Capintec, Ramsey, US) was determined. k_Q is determined by the mean restricted mass collision stopping power ratio of the medium to air $(\overline{L}/\rho)_{m,air}$ and the overall perturbation factor P. $(\overline{L}/\rho)_{m,air}$ was calculated for several slab compensator thicknesses using the SPRRZnrc code [17–19]. The calculation was performed for water and each chamber wall material. In the calculation, cutoff energy was set at AE = ECUT = 0.521 MeV, AP = PCUT = 0.01 MeV. P consists of the wall correction factor P_{wall}, scattering differences between the air cavity and the water correction factor P_{cav}, the central electrode correction factor P_{cel} and the displacement factor P_{dis}. P_{cav}, P_{cel} and P_{dis} were determined by the method adopted as the Japanese Society of Medical Physics (JSMP) Standard Dosimetry 01 [20–24]. P_{wall} was determined by the following equation [25–27]:

$$(P_{wall})_Q = \frac{\alpha\left(\frac{\overline{L}}{\rho}\right)_{wall,air}\left(\frac{\overline{\mu}_{en}}{\rho}\right)_{w,wall} + \tau\left(\frac{\overline{L}}{\rho}\right)_{sleeve,air}\left(\frac{\overline{\mu}_{en}}{\rho}\right)_{w,sleeve} + (1-\alpha-\tau)\left(\frac{\overline{L}}{\rho}\right)_{w,air}}{\left(\frac{\overline{L}}{\rho}\right)_{w,air}} \quad [1]$$

Where α and τ are the ratios of the electrons generated from the chamber wall and the sleeve, respectively. Those values were determined from the experimental value of Lempert *et al.* [28]. $(\overline{\mu}_{en}/\rho)_{w,med}$ is the mean mass energy absorption coefficient ratio of water to medium and is determined by the following equation:

$$\left(\frac{\overline{\mu}_{en}}{\rho}\right)_{w,med} = \frac{\int_0^{E_{max}} \Phi_E E\,(\mu_{en}(E)/\rho)_w\,dE}{\int_0^{E_{max}} \Phi_E E\,(\mu_{en}(E)/\rho)_{med}\,dE} \quad [2]$$

Where Φ_E is the photon fluence at energy E in water, and the dataset of Seltzer and Hubbell [29, 30] was applied for $(\mu_{en}(E)/\rho)$.

Head scatter factor measurement and scattered photon simulation.

To evaluate the influence on head scatter factor S_h by scattered photons generated within the compensator, S_h values for several slab compensator thicknesses were determined by measurement of in-air output. Measurement was performed using the Farmer-type ionization chamber (TM30013, PTW, Freiburg, Germany) in combination with

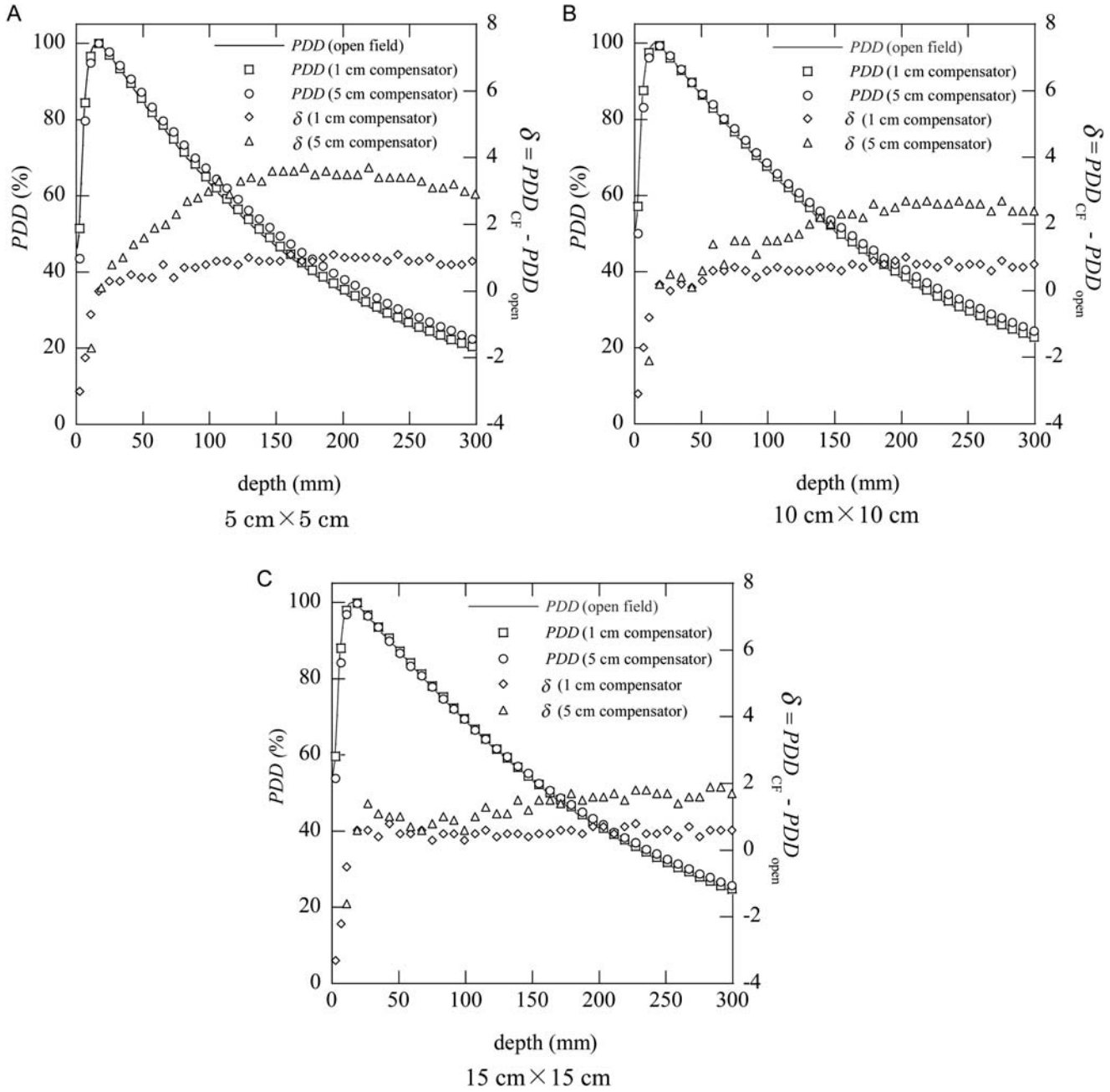

Fig. 1. Comparison between *PDD* of open field and that of compensator field. (**A**) 5 cm × 5 cm field; (**B**) 10 cm × 10 cm field; (**C**) 15 cm × 15 cm field.

an electrometer (Unidos, PTW). The chamber was positioned at 10 cm depth in the miniphantom, which had a cylindrical shape with a 2-cm radius and was 20 cm in height, and these were placed at SCD = 100 cm on the beam axis. S_h was determined as the ratio of in-air output of an arbitrary field to that of a 10 cm × 10 cm reference field [31].

In order to evaluate the contribution of the scattered photons generated within the compensator to in-air output, fluence of primary and scattered photons in air were simulated for several field sizes and compensator thicknesses using the Monte Carlo method. The Monte Carlo simulation parameters were same as in the above section. Scattered photons generated within the compensator were identified by the latch option. The collision water kerma for the arbitrary field ${}_{\mathrm{col}}K_{\mathrm{water}}(A)$ was calculated using the following equation:

$$ {}_{\mathrm{col}}K_{\mathrm{water}}(A) = \int_{E_{\min}}^{E_{\max}} \Phi_E(A)\, E\, \frac{\mu_{\mathrm{en}}}{\rho}\, \mathrm{d}E \qquad [3] $$

Where Φ_E (A) is photon fluence at energy E for field size A, and $\mu_{en}(E)/\rho$ is the mass energy absorption coefficient of water, respectively.

RESULTS AND DISCUSSION

Percentage depth dose

Figure 1 shows a comparison between the *PDD* of the open field and that of the compensator field. For a 5-cm compensator and at 10 cm depth, deviations of *PDD* δ were 3.3%, 1.7% and 1.1% higher than *PDD* for 5 cm × 5 cm, 10 cm × 10 cm and 15 cm × 15 cm open field, respectively. When X-rays passed the compensator, the depth dose was increased by the beam hardening effect, and this phenomenon is obvious for smaller fields.

Figure 2 shows a comparison of the photon energy spectrum between the open and 5-cm compensator field. In air, the mean photon energy was 1.72 MeV and 2.42 MeV for the 5 cm × 5 cm field, and 1.68 MeV and 2.21 MeV for the 15 cm × 5 cm field, respectively. When under the 5-cm compensator, the fluence of low energy photons decreased and mean energy shifted to higher. This result shows beam hardening was obviously taking place in the compensator, but the variation of the energy spectrum by field size was insignificant in air. On the other hand, in water, the mean photon energy was 2.23 MeV and 1.59 MeV for 5 cm × 5 cm and 15 cm × 15 cm compensator fields, respectively. For smaller fields, the energy spectrum for the compensator field had no change whether in water or air, and there was an obvious difference between the photon spectrum in water of the open field and the compensator field. However for larger fields, the fluence of low energy photons generated within water was increased and the energy spectrum of compensator field was similar to the open field. This phenomenon explains why variation of *PDD* was larger for smaller fields.

In order to obtain high accuracy of dose calculation for the compensator IMRT, the energy spectrum should be reproduced correctly.

Beam quality correction factor k_Q

Figure 3 shows the variation of mean restricted mass collision stopping power ratio of medium to air $(\overline{L}/\rho)_{m,air}$ as a function of compensator thickness. As compensator thickness increased, $(\overline{L}/\rho)_{m,air}$ decreased in every material. For the 5-cm compensator, the deviation of $(\overline{L}/\rho)_{water,air}$ from the open field was 0.5%. This result shows beam hardening may affect beam quality correction factor k_Q.

Figure 4 shows the variation of k_Q as a function of compensator thickness. As compensator thickness increased, k_Q for all Farmer-type ionization chambers decreased, and the difference of k_Q between the open and 5-cm compensator fields was 0.45%. Although the k_Q of Farmer-type ionization chamber could be varied because of beam hardening, the variation was in the range of uncertainty of k_Q determination [20, 21].

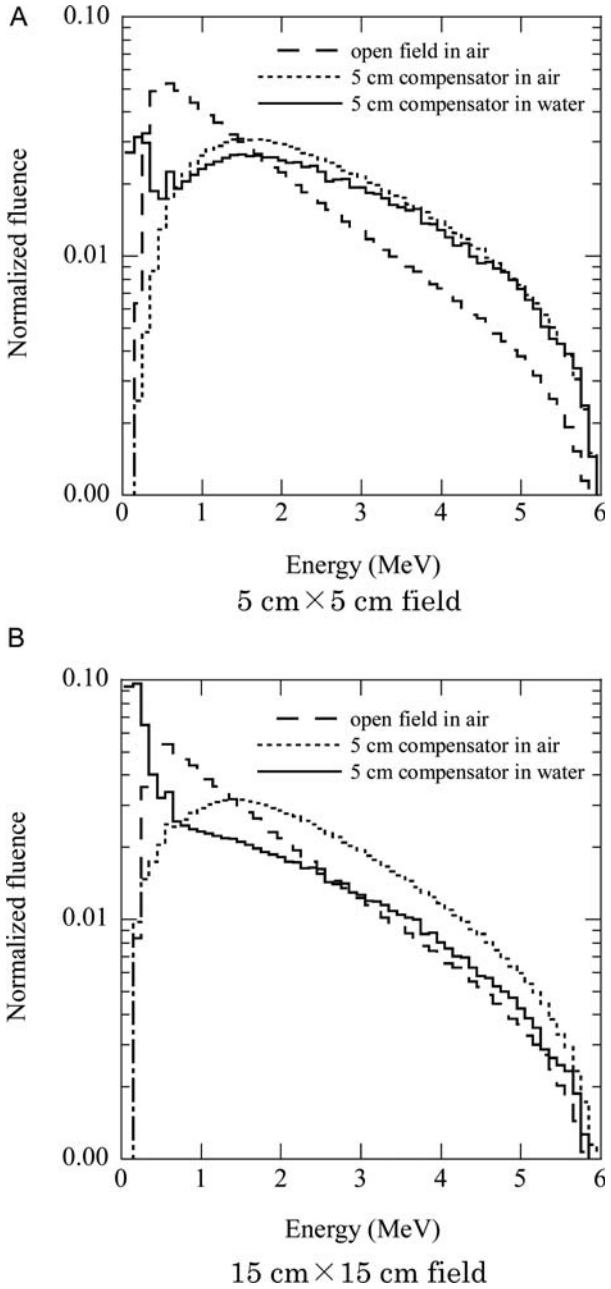

Fig. 2. Comparison of photon energy spectrum between open and 5 cm compensator field (**A**) 5 cm × 5 cm field; (**B**) 15 cm × 15 cm field.

Head scatter factor S_h

Variation of S_h for several compensator thicknesses is shown in Fig. 5. When compensator thickness increased, S_h has a steeper gradient. This result shows dose output may be affected by the scattered photons generated within the compensator.

Figure 6 shows the ratio of ${}_{col}K_{water}$ of simulated scattered photons generated within the compensator to total scattered photons for several compensator thicknesses. The contribution of the scattered photons generated within the

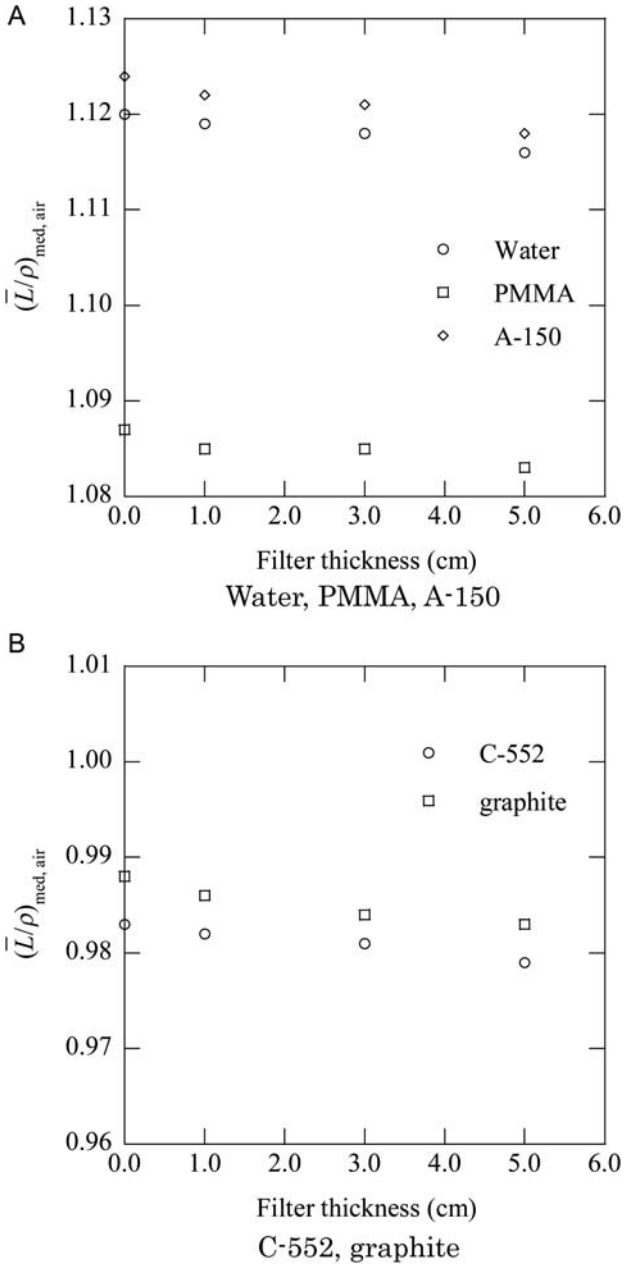

Fig. 3. Variation of mean restricted mass collision stopping power ratio of medium to air $(\bar{L}/\rho)_{m,air}$ as a function of filter thickness. (**A**) Water, PMMA, A-150; (**B**) C-552, graphite.

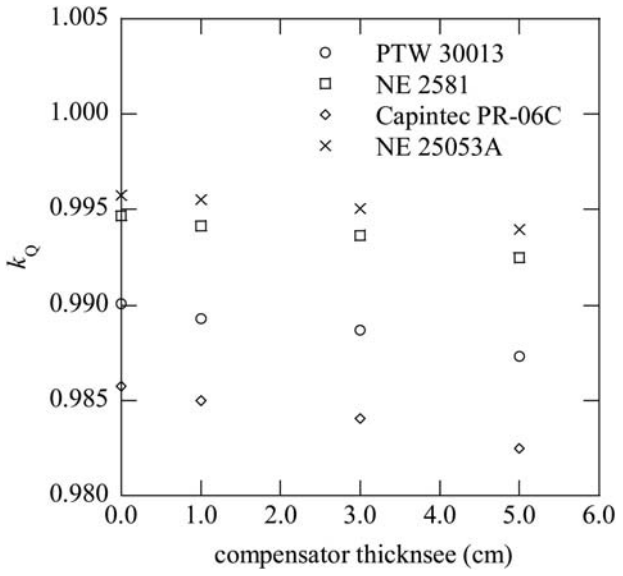

Fig. 4. Variation of beam quality correction factor as a function of compensator thickness.

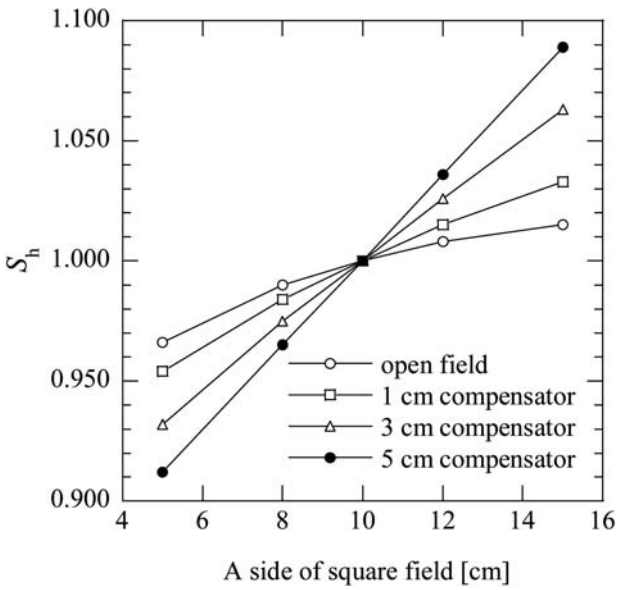

Fig. 5. Variation of head scatter factor for several compensator thicknesses.

compensator increases when the field size and compensator thickness increases. Therefore, the scattered photons generated within the compensator should be taken into account in the MU calculation of compensator IMRT.

CONCLUSION

In this report, the influence of a brass compensator on dose calculation and dosimetry was investigated. As a result, when the photon passed the brass compensator, beam hardening occurred, and dose distribution was varied with the compensator. Furthermore, scattered photons were generated within the compensator, and scattered photons affect the head scatter factor. Figure 7 shows the MU calculation difference at 10 cm depth without energy spectrum reproduction and correction of scattered photons for head scatter factor. When the energy spectrum reproduction and correction

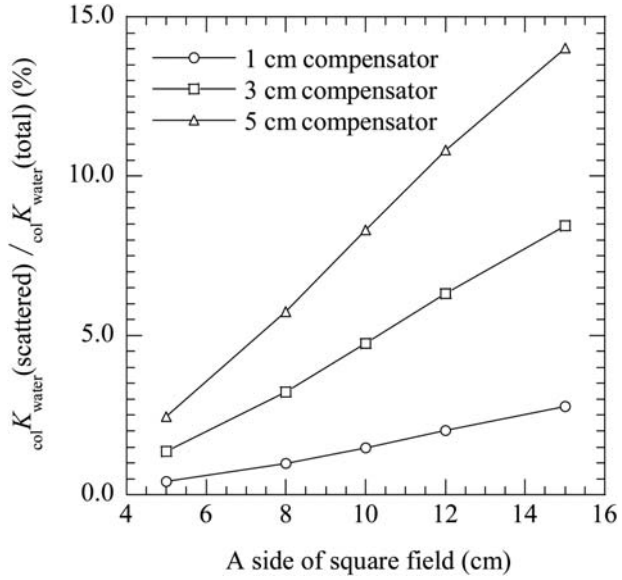

Fig. 6. Percentage of collision water kerma of scattered photons from compensator to that of total photons for several compensator thicknesses.

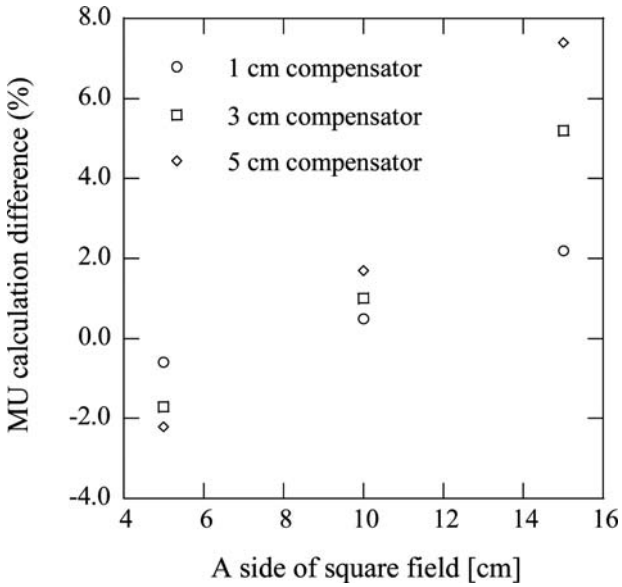

Fig. 7. MU calculation difference at 10 cm depth without energy spectrum reproduction and correction of scattered photons for head scatter factor.

of S_h are not included in the MU calculation, the MU difference is up to 7%. This means that energy spectrum should be reproduced correctly and scattered photons must be taken into account for accurate dose calculation for the brass compensator IMRT. On the other hand, influence of beam hardening on k_Q was insignificant.

REFERENCES

1. Boyer AL, Butler EB, DiPetrillo TA *et al*. Intensity-modulated radiotherapy: current status and issues of interest. *Int J Radiation Oncology Biol Phys* 2001;**51**:880–914.
2. Boyer AL, Xing L, Xia P., Beam shaping, intensity modulation. In: Van Dyk J (ed.) *The Modern Technology of Radiation Oncology*. pp. 454–455. Madison, WI: Medical Physics Publishing, 2001.
3. Chang SX, Cullip TJ, Deschesne KM. Intensity modulation delivery techniques: 'step & shoot' MLC auto-sequence versus the use of a modulator. *Med Phys* 2000;**27**:948–59.
4. Williams PC. IMRT delivery techniques and quality assurance. *Br J Radiol* 2003;**76**:766–76.
5. Bouchard H, Seuntjens J, Carrier JF *et al*. Ionization chamber gradient effects in nonstandard beam configurations. *Med Phys* 2009;**36**:4654–62.
6. Fujita Y, Tohyama N, Saitoh S *et al*. Depth scaling of solid phantom for intensity modulated radiotherapy beams. *J Radiant Res* 2010;**51**:707–13.
7. LoSasso T, Chui CS, Ling CC. Physical and dosimetric aspects of a multileaf collimation system used in the dynamic mode for implementing intensity modulated radiotherapy. *Med Phys* 1998;**25**:1919–27.
8. Low DA, Son JW, Klein EE *et al*. Characterization of a commercial multileaf collimator used for intensity modulated radiation therapy. *Med Phys* 2001;**28**:752–6.
9. LoSasso T, Chui CS, Ling CC. Comprehensive quality assurance for the delivery of intensity modulated radiotherapy with a multileaf collimator used in the dynamic mode. *Med Phys* 2001;**28**:2209–19.
10. Xia P, Chuang CF, Verhey LJ. Communication and sampling rate limitations in IMRT delivery with a dynamic multileaf collimator system. *Med Phys* 2002;**29**:412–23.
11. Ezzell GA, Chungbin S. The overshoot phenomenon in step-and-shoot IMRT delivery. *J Appl Clin Med Phys* 2001; **2**:138–48.
12. Oguchi H, Obata Y. Commissioning of modulator-based IMRT with XiO treatment planning system. *Med Phys* 2009;**36**:261–9.
13. Nelson WR, Hirayama H, Rogers DWO. The EGS4 Code System, SLAC Report No. SLAC-265, 1985
14. Rogers DWO, Faddegon BA, Ding GX *et al*. A Monte Carlo code to simulate radiotherapy treatment units. *Med Phys* 1995;**22**:503–24.
15. Kawrakow I, Rogers DWO. The EGSnrc Code System: Monte Carlo Simulation of Electron and Photon Transport, NRCC Report No. PIRS-701. 23–94, 2003.
16. Fujita Y, Saitoh H, Myojoyama A. Bremsstrahlung and photoneutron leakage from steel shielding board impinged by 12-24 MeV electron beams. *J Radiant Res* 2009;**50**:363–9.
17. Rogers DWO, Kawrakow I, Seuntjens JP *et al*. NRC User Codes for EGSnrc, NRCC Report No. PIRS-702 revB, 2003, 60–62.
18. Nahum AE. Water/air stopping-power ratios for megavoltage photon and electron beams. *Phys Med Biol* 1978;**23**:24–38.
19. Malamut C, Rogers DWO, Bielajew AF. Calculation of water/air stopping-power ratios using EGS4 with explicit

treatment of electron positron differences. *Med Phys* 1991; **18**:1222–8.
20. JSMP. *Standard Dosimetry of Absorbed Dose in External Beam Radiotherapy*. Standard Dosimetry 01. Tokyo: Tsusho-Sangyo-Kenkyu-Sha, 2002 (in Japanese)
21. IAEA. Absorbed dose determination in external beam radiotherapy – An international code of practice for dosimetry based on standards of absorbed dose to water. Code of practice for high energy electron beams. TRS-398. Vienna: IAEA, 2004.
22. AAPM. Protocol for clinical dosimetry of high-energy photon and electron beams. *Med Phys* 1999;**26**:1847–70.
23. Ma CM, Nahum AE. Effect of the size and composition of the central electrode on the response of cylindrical ionization chambers in high-energy photon and electron beams. *Phys Med Biol* 1993;**38**:267–90.
24. Palm A, Mattsson O. Experimental study on the influence of the central electrode in Farmer-type ionization chambers. *Phys Med Biol* 1999;**44**:1299–308.
25. Almond PR, Svensson H. Ionization chamber dosimetry for photon and electron beams theoretical considerations. *Acta Radiol Ther Phys Biol* 1977;**16**:177.
26. Gillin MT, Kline RW, Niroomand-Rad A., Grimm DF. The effect of thickness of the waterproofing sheath on the calibration of photon and electron beams. *Med Phys* 1985;**12**: 234–6.
27. Hanson WF, Tinoco JAD. Effects of plastic protective caps on the calibration of therapy beam in water. *Med Phys* 1985;**12**:
243–8.
28. Lempert GD, Nath R, Schulz RJ. Fraction of ionization from electrons arising in the wall of an ionization chamber. *Med Phys* 1983;**10**:1–3.
29. Seltzer SM. Calculation of photon mass energy-transfer and mass energy-absorption coefficients. *Radiat Res* 1993;**136**: 147–70.
30. Hubbell JH. Photon mass attenuation and energy-absorption coefficients from 1 keV to 20 MeV. *Int J Appl Radiat Isot* 1982;**33**:1269–90.
31. Timothy CZ, Anders A, Kwok LL *et al*. Report of AAPM Therapy Physics Committee Task Group 74: In-air output ratio, S_c, for megavoltage photon beams. *Med Phys* 2009;**36**:5261–91.